

Variability of Be Stars in Southern Open Clusters

M. Virginia McSwain^{1,2}

*Department of Physics, Lehigh University, 16 Memorial Drive East, Bethlehem, PA 18015;
mcswain@lehigh.edu*

Wenjin Huang

*Department of Astronomy, University of Washington, Box 351580, Seattle, WA 98195-1580;
wenjin@astro.washington.edu*

Douglas R. Gies

Center for High Angular Resolution Astronomy, Department of Physics and Astronomy, Georgia State University, P.O. Box 4106, Atlanta, GA 30302-4106; gies@chara.gsu.edu

ABSTRACT

We recently discovered a large number of highly active Be stars in the open cluster NGC 3766, making it an excellent location to study the formation mechanism of Be star disks. To explore whether similar disk appearances and/or disappearances are common among the Be stars in other open clusters, we present here multiple epochs of H α spectroscopy for 296 stars in eight open clusters. We identify 12 new transient Be stars and confirm 17 additional Be stars with relatively stable disks. By comparing the H α equivalent widths to the photometric y -H α colors, we present a method to estimate the strength of the H α emission when spectroscopy is not available. For a subset of 128 stars in four open clusters, we also use blue optical spectroscopy and available Strömgen photometry to measure their projected rotational velocities, effective temperatures, and polar surface gravities. We combine our Be star detections from these four clusters to investigate physical differences between the transient Be stars, stable Be stars, and normal B-type stars with no line emission. Both types of Be stars are faster rotating populations than normal B-type stars, and we find no significant physical differences between the transient and stable Be stars in our sample.

Subject headings: stars: emission-line, Be — open clusters and associations: individual (NGC 3293, NGC 3766, NGC 4755, NGC 6231)

1. Introduction

Classical Be stars are a class of B-type stars with circumstellar disks that cause Balmer and other line emission. As a population, they rotate faster than their nonemission, B-type counterparts with a rotational velocity comparable to the crit-

ical velocity (Hunter et al. 2008; Martayan et al. 2006; Martayan et al. 2007). There are three possible reasons for the rapid rotation of Be stars: they may have been born as rapid rotators, spun up by binary mass transfer, or spun up during the main-sequence (MS) evolution of B stars. The rotation is likely combined with weaker processes, such as nonradial pulsations (NRPs) or magnetic fields to move material from the stellar surface into the disk (Porter & Rivinius 2003).

We began studying the Be phenomenon in open

¹Visiting Astronomer, Cerro Tololo Inter-American Observatory. CTIO is operated by AURA, Inc. under contract to the National Science Foundation.

²NSF Astronomy and Astrophysics Postdoctoral Fellow

clusters with a photometric and spectroscopic investigation of NGC 3766 (McSwain & Gies 2005a; hereafter Paper 1). We then applied our photometric technique to perform a survey of 55 southern open clusters to examine the Be star ages and dependence on main-sequence and post-main-sequence evolution (McSwain & Gies 2005b; hereafter Paper 2). With 52 definite Be star detections and 129 Be candidates identified in that survey, our results indicated that the fraction of Be stars in a cluster increases with age until 100 Myr. Be stars are most common among the brightest, most massive B-type stars above the zero-age MS (ZAMS). A spin-up phase at the terminal-age MS (TAMS) cannot produce the observed distribution of Be stars, but up to 73% are consistent with spin-up by mass transfer in a close binary system. Most of the remaining Be stars were likely rapid rotators at birth. Other recent surveys of Be stars in Galactic and Magellanic Cloud open clusters have found similar results (Wisniewski & Bjorkman 2006; Mathew et al. 2008).

During a followup spectroscopic study of the cluster NGC 3766 (McSwain et al. 2008; hereafter Paper 3), we discovered unprecedented activity among its Be stars. Between 2003–2007, we observed disk appearances and/or near disappearances in 11 of its 16 Be stars. The observed disk formation rates implied a very slow equatorial surface flow on average, but the surface flow can be an order of magnitude faster at times. Our measurements of the changing disk sizes in NGC 3766 are consistent with the idea that transitory, nonradial pulsations contribute to the formation of these highly variable disks.

One of the primary motivations of this work was to confirm many of our Be candidates from Paper 2 with spectroscopic observations and improve the fraction of known Be stars in southern open clusters. We also sought to discover additional Be stars that exhibit frequent changes in their disk states, transitioning between the Be and “normal” B-type spectra, as we observed among most of the Be stars in NGC 3766. Finally, spectroscopic observations allow us to probe the rotational velocities and other physical parameters that may distinguish Be stars from non-emitting B-type stars.

Throughout this work, we adopt the term “transient Be stars” to describe any Be star ob-

served in both the Be and normal B-type spectroscopic states. Likewise, we use the term “stable Be stars” to describe Be stars whose disks are present in all observations, even though the strength of the disk emission may change dramatically.

Here we present multiple epochs of H α spectroscopy of eight open clusters, and we identify 12 previously unknown transient Be stars from this sample. We also confirm 17 additional Be stars that have relatively stable disks. For a subset of four open clusters, we also present blue optical spectroscopy and measurements of the effective temperature, T_{eff} , surface gravity, $\log g$, and projected rotational velocity, $V \sin i$. Combining these results with our previous measurements of members of NGC 3766, we compare the total samples of transient Be stars, stable Be stars, and normal B-type stars to explore physical differences in these three populations. Other than the temporary disappearance of their disk emission, we find no physical differences between transient Be stars and the Be stars with relatively stable disks.

2. Observations

We obtained red optical spectra of 296 Be and B-type stars in 8 open clusters during observing runs in 2005 February, 2006 May, and 2007 May using the CTIO Blanco 4-m telescope with the Hydra multi-fiber spectrograph. For a subset of 4 open clusters, we also obtained blue optical spectra during the 2006 and 2007 runs. The spectrograph setups differed slightly between all these runs, and the details are summarized in Table 1. We used slit plates and/or order-sorting filters in some of our observing runs, and when either was not used, Table 1 contains a null value.

We selected the targets for each run by giving highest priority to the known Be stars in the cluster. We then selected other B-type stars in the cluster by ranking them according to their y -H α color to preferentially select any weak emission, Be star candidates from our photometry (Paper 2). In Paper 3, we published results from 47 members of NGC 3766, and we here we expand that sample with red and blue spectra of 10 additional members observed in 2007 May. Also in Paper 3, four Be stars did not have available blue spectra to measure their $V \sin i$, and we included them in the new target list. For the other clusters, we used

the same fiber assignments to achieve a target list as consistent as possible, but a broken fiber prohibited a few stars from being observed in later runs. Also, the 2007 blue spectra suffered from much lower signal-to-noise ratios (S/N) due to the slit plate inserted in front of the fibers (possibly misaligned and blocking light), so several targets from this configuration were excluded from our measured sample.

We generally began the Hydra observations by taking short exposures and then parking the fibers used for the brightest stars to avoid saturation in longer exposures of 1800 s. Therefore we usually obtained up to 5–7 exposures of each star. We also observed a HeNeAr comparison lamp source just before and after each set of cluster observations for wavelength calibrations.

All of the spectra were zero corrected using standard routines in IRAF, and they were flat fielded, wavelength calibrated, and sky subtracted in IRAF using the *dohydra* routine. Of the 7 clusters observed, only NGC 3293 and IC 2581 had widespread nebulosity that was difficult to remove completely during the sky subtraction. The effect was pronounced in the $H\alpha$ line in our red spectra, but the nebulosity presented much less of a problem in the $H\gamma$ and other Balmer lines in our blue spectra. For each set of Hydra spectra, we transformed the observations to a common heliocentric wavelength grid, co-added them to achieve good S/N for each star, and rectified the total spectrum to a unit continuum.

3. Be Star Variability and $H\alpha$ Equivalent Widths

In Paper 3, we reported the discovery of 11 transient Be stars in NGC 3766 whose disks appeared and/or nearly completely disappeared during our 4 years of observations. Only five of the observed Be stars had relatively consistent disks during the same period. It turns out that NGC 3766 is not the only cluster containing such variable Be stars; during two or three epochs of red spectroscopy, we have discovered many new transient Be stars in nearly every cluster reported here. The $H\alpha$ profiles of each Be star are shown in Figures 1–3.

We measured the equivalent widths of the $H\alpha$ line profiles, $W_{H\alpha}$, by directly integrating across

each rectified spectrum over the range 6535–6591 Å to include the broad wings expected for this strong line. The error in $W_{H\alpha}$ is about 10% due to noise in the continuum regions. We use the convention that a pure absorption line has a positive equivalent width. Many authors prefer to investigate Be emission strength by subtracting the photospheric absorption line profile and measuring $W_{H\alpha}$ from the net emission profile only. We avoid that here for two reasons: we would like to compare the raw $W_{H\alpha}$ for both emission line and non-emission line stars to their photometric colors, and we do not know an accurate photospheric line strength without knowing the effective temperature and gravity of the stars. We measure these stellar properties below for a subset of our targets, but for consistency, we present only the raw $W_{H\alpha}$ for all stars.

The resulting $W_{H\alpha}$ are listed in Table 2, columns 2–4. In column 5, we also identify the Be stars and candidates found in our photometry (Paper 2). Finally in column 6, we list the Be star status based upon our red spectroscopic observations only. While the photometric method is often unsuccessful identifying small or transient disks, it is usually very accurate when identifying strong emitters. Only three stars were identified as Be in Paper 2 that are not confirmed here: Collinder 272-565, NGC 4755-43, NGC 6231-67. We argue below that the first is likely a foreground star; the latter two may be Be transients that have not yet been confirmed spectroscopically.

Several Be stars exhibit dramatic changes in their disk states, alternately showing strong disk emission and a near complete disappearance of the disk: Collinder 272-562, Collinder 272-621, Hogg 16-185, NGC 3293-83, NGC 4755-18, and NGC 4755-31. Normal B-type stars are not expected to have strong stellar winds with emission forming in the $H\alpha$ line, so any weak emission partially filling in the line or the wings is more likely due to a very small Be disk. Several stars show line profile variations consistent with weak disks during one or more observations: Collinder 272-767, NGC 3293-74, NGC 6231-2, NGC 6231-90, and NGC 6231-221. Finally, the star IC 2581-113 appears to have a transient shell profile, indicating absorption through an edge-on disk. We classify all 12 of these stars as Be transients. Seven of these transient Be stars have available blue spec-

tra, and combined with the 11 transient Be stars observed in NGC 3766, we have a large sample to compare the transient population with stable Be stars, discussed below.

An additional 17 Be stars exhibit line emission from their disks that are present in all of our observations, yet these “stable” disks vary in $W_{H\alpha}$ just as much or more than the transient disks. In Paper 3, we found very similar mass gain and mass loss rates for the disks among all of the Be stars, suggesting similar origins for all of the disks. The Be stars presented here have variability properties that are highly consistent with those observed in NGC 3766.

In total, we have identified 29 Be stars from our $H\alpha$ spectroscopy of Collinder 272/Hogg 16, IC 2581, NGC 3293, NGC 4755, NGC 6231, and NGC 6664, as well as 16 Be stars in NGC 3766 (Paper 3). Based on multiple epochs of $H\alpha$ spectroscopy for most of these 45 Be stars, we present lower limits of each cluster’s transient Be star fraction in Table 3. Here, we calculate the percentage, p , of transient Be stars, t , compared to the total number of Be stars, n , using

$$p = \frac{t}{n}. \quad (1)$$

Although the total populations of Be stars in each cluster are relatively small, the standard error associated with this fraction of transients is approximately given by the root of the variance for a binomial distribution,

$$\sigma_p \approx \sqrt{\frac{p(1-p)}{n}}. \quad (2)$$

For NGC 6664, this standard error should be zero since $p = 0$. However, we find a more realistic error by allowing p to vary until $\sigma_p \approx p$. The Poisson errors associated with t and n are \sqrt{t} and \sqrt{n} respectively. The clusters Collinder 272/Hogg 16, NGC 3766, and NGC 6231 have the highest rates of variable Be star disks.

Meilland et al. (2006) discuss two mechanisms that may account for our observed transitions from the Be to B spectroscopic phases: discrete mass loss outbursts that form expanding ring-like structures around the star, and continuous mass loss that slowly decreases in magnitude and allows the disk to dissipate. Based on our measurements of

the changing disk masses in both stable and transient Be stars (Paper 3), we favor the first scenario. In that work, we measured mass gain rates for the disks that appear to increase by an order of magnitude during short time intervals. However, our spectra are not of sufficient resolving power to prove whether the emission lines evolve according to the ring scenario. Higher resolution spectra will determine whether the peak separation in the emission lines remains constant while the high velocity wings disappear, as Meilland et al. (2006) predict for such a discrete mass loss scenario.

In Paper 1, we showed that in NGC 3766, the observed $W_{H\alpha}$ and $y-H\alpha$ colors have an approximately logarithmic relationship according to

$$y - H\alpha = C + 2.5 \log \frac{FWHM - W_{H\alpha}}{FWHM}, \quad (3)$$

where $FWHM$ is the range covered by the narrowband $H\alpha$ filter and C is a constant. Using our mean observed $W_{H\alpha}$ presented in Table 2 and the $y-H\alpha$ colors from Paper 2, we have performed a similar fit for each cluster presented here. The resulting fitting constants C for each cluster are summarized in Table 4, and the adjusted colors $y-H\alpha - C$ for all stars with measured $W_{H\alpha}$ are plotted in Figure 4. The observed ranges in $W_{H\alpha}$ are shown with horizontal error bars. Since $W_{H\alpha}$ is highly variable even among the stable Be stars, most of the scatter in this plot is explained by the time separation between our photometric and spectroscopic observations. Some additional scatter is expected since the disks likely vary in density, opacity, and inclination. The outlying star with $W_{H\alpha} = 10 \text{ \AA}$ (Collinder 272-565) is either a transient Be star or a foreground star (more likely since transient Be stars usually have bluer $y-H\alpha$ colors due to their smaller, temporary disks).

Since reddening affects the continuum flux measured over the intermediate-band y filter more than the narrow-band $H\alpha$ filter, the constant C is dependent on the cluster’s reddening, $E(b-y)$. It will also depend upon the absolute scale of the $H\alpha$ magnitude. We show in Figure 5 that for our calibration of $y-H\alpha$, there is a direct relationship between C and $E(b-y)$. We find a linear fit

$$C = (0.97 \pm 0.12)E(b-y) + (0.14 \pm 0.04) \quad (4)$$

between the two parameters. Since spectroscopy is often unavailable in many observing programs, it

is thus possible to estimate $W_{H\alpha}$ of a Be star from its photometric properties $y-H\alpha$ and $E(b-y)$. A simple radiative transfer model such as that of Grundstrom & Gies (2006) may then be applied to investigate the physical size of the disk. However, due to the large scatter in the observed relations we caution that absolute disk measurements are very imprecise and only differential changes in $y-H\alpha$ should be applied to estimate first-order changes in the disk’s extent. Since the $H\alpha$ filter system is not universally standard, different filters or photometric calibrations may produce a slightly different relationship between C and $E(b-y)$ that must be determined before estimating $W_{H\alpha}$.

4. Physical Parameters of Stars

In Paper 3, we presented the physical parameters of 38 Be and B-type stars in NGC 3766 measured from blue optical spectra. Here, we present measurements for additional members of NGC 3766 and three other clusters, for a total blue sample of 128 Be and B-type stars. The blue sample includes only 17 of the transient Be stars and 12 of the stable Be stars, and we discuss the measurements of $V \sin i$, T_{eff} , and $\log g_{\text{polar}}$ below.

4.1. $V \sin i$ Measurements

Our technique for measuring $V \sin i$ for B-type stars is described in detail in Paper 3. In short, we generated a grid of model spectra using SYNSPEC (Lanz & Hubeny 2003) and Kurucz ATLAS9 atmospheric models (Kurucz 1994) assuming plane-parallel geometry and local thermodynamic equilibrium (LTE). We also adopted solar abundances and a microturbulent velocity of 2 km s^{-1} for all stars. For each star, we made a preliminary estimate of its effective temperature and gravity, T_{eff} and $\log g$ respectively, by comparing the observed $H\gamma$, $H\delta$, and He I line profiles to our grid of Kurucz spectral models. To measure $V \sin i$, we compared the observed He I $\lambda 4388$ and He I $\lambda 4471 + \text{Mg II } \lambda 4481$ line profiles to the model profiles convolved with a limb-darkened, rotational broadening function and a Gaussian instrumental broadening function. We determined the best fit over a grid of values by minimizing the mean square of the deviations, rms^2 . The formal error, $\Delta V \sin i$, is the offset from the best-fit value that increases the rms^2 by $2.7 \text{ rms}^2 / N$, where N is the

number of wavelength points within the fit region. Our measured $V \sin i$ and $\Delta V \sin i$ are listed in columns 3–4 of Table 5.

In nearly all of the Be stars in our sample, the He I lines do not exhibit obvious signs of emission. These lines are, in general, much less susceptible to emission than the $H\gamma$ or $H\delta$ lines. Nevertheless, we consider our $V \sin i$ measurements for Be stars to be lower limits since the He I lines may contain some weak emission in Be stars, partially filling and narrowing their line profiles. On the other hand, those clusters with strong nebular emission may have weak He I emission that may cause these lines to appear more shallow, hence resulting in an overestimate of $V \sin i$.

We compared our measured $V \sin i$ to the measurements available for each cluster in the WEBDA database¹. The agreement is generally good, although we find a large scatter due to the systematic differences among authors. For 18 stars, WEBDA lists $V \sin i$ measurements from multiple sources. The differences between our measurements and WEBDA is comparable to the differences between the various sources. We measured the standard deviation, $\sigma_{V \sin i}$, of the difference between our measurements and the literature to be 25.7 km s^{-1} . Stars with more than $3\sigma_{V \sin i}$ difference in $V \sin i$ are probably unresolved double lined spectroscopic binaries (SB2s), and we find three new SB2 candidates in our sample: NGC 3293–27, NGC 6231–132, and NGC 6231–137. We note that García & Mermilliod (2001) argue that NGC 6231–132 is an SB1 with a period of 8.9 d and that NGC 6231–137 is a β Cep star and a probable SB1. These and other spectroscopic binaries identified by blended lines in our spectra or by classification in the literature are identified in column 15 of Table 5.

4.2. T_{eff} and $\log g$ Measurements of B stars

We measured T_{eff} and $\log g$ for each B-type star using the technique described in Paper 3, and we summarize the procedure here. For the coolest stars with $T_{\text{eff}} < 15,000 \text{ K}$, we used the “virtual star” method of Huang & Gies (2006), which assumes a spherically symmetric geometry

¹The WEBDA database is maintained by J.-C. Mermilliod and is available online at <http://obswww.unige.ch/webda/navigation.html>.

and constant T_{eff} and $\log g$ across the stellar surface. They generated detailed $\text{H}\gamma$ line profiles using line-blanketed, LTE Kurucz ATLAS9 and SYNSPEC codes. Huang & Gies show that the $\text{H}\gamma$ wing strength and line equivalent width can be used as starting parameters in a line profile fit to obtain unique values of T_{eff} , $\log g$, and their corresponding errors.

To measure the hotter B-type stars, we used the new TLUSTY BSTAR2006 grid of metal line-blanketed, non-LTE, plane-parallel, hydrostatic model spectra (Lanz & Hubeny 2007). We used their models with solar metallicity and helium abundance and a microturbulent velocity of 2 km s^{-1} . We compared the $\text{H}\gamma$ line profile to the rotationally and instrumentally broadened model spectral line profiles at each value in the grid, minimizing rms^2 across the line region. We then refined our measurements to a higher precision using a linear interpolation between the available line profiles in the grid. Finally, we determined the errors, ΔT_{eff} and $\Delta \log g$, from the values which produce a rms^2 no more than $2.7 \text{rms}^2/N$ greater than the minimum rms^2 . Our measurements of T_{eff} and $\log g$, with their corresponding errors, are listed in columns 5–8 of Table 5.

For stars with T_{eff} near 15,000 K, we measured the parameters using both methods. Since the method of Huang & Gies can be applied to the hotter stars (although it does not include non-LTE effects), it is an appropriate tool to compare with TLUSTY in this temperature regime. We find very good agreement from both methods, and we adopt the TLUSTY results here.

A few stars in NGC 3293 were contaminated by nebulosity in the $\text{H}\gamma$ line, manifested as a narrow emission profile in the line core. To measure T_{eff} and $\log g$ for these stars, we omitted the center 5–6 Å of the line profile in our fits and used only the broader wings.

Rapidly rotating B stars may be distorted into an oblate spheroidal shape, so the surface gravity at the equator can be much lower than at the poles, and this $\log g_{\text{polar}}$ is a better indicator of the evolutionary state of the star. Huang & Gies (2006) performed detailed spectroscopic modeling of such distorted rotating stars to determine a statistical correction factor for $\log g$, averaged over all possible i , for a variety of stellar models. We made a bilinear interpolation between their mod-

els to convert our measured $\log g$ to $\log g_{\text{polar}}$ for a more accurate comparison between slow and rapid rotators.

For each B star, we also measured its mass, M_* , and radius, R_* , by interpolating between the evolutionary tracks for non-rotating stars from Schaller et al. (1992). The errors ΔM_* and ΔR_* correspond to our measured ΔT_{eff} and $\Delta \log g$. For simplicity, we assume the polar radius of the star, R_p is equal to R_* , and a rotationally distorted star has an equatorial radius $R_e = 1.5R_p$ in the Roche approximation. The resulting critical velocity is

$$V_{\text{crit}} = \sqrt{\frac{GM_*}{R_e}}. \quad (5)$$

Our results for $\log g_{\text{polar}}$, M_* , ΔM_* , R_* , and ΔR_* , and V_{crit} are also listed in Table 5, columns 9–14.

4.3. T_{eff} and $\log g$ Measurements of Be stars

We measured T_{eff} and $\log g$ for the Be stars using available Strömgren m_1 , c_1 , and β indices for our targets, available from the WEBDA database, as described in Paper 3. To determine the dereddened indices, we adopted the reddening, $E(b-y)$, listed in Table 4. We used the relation

$$E(b-y) = 0.745 E(B-V) \quad (6)$$

to relate $E(b-y)$ and $E(B-V)$ when the latter was given in the literature. In Paper 3, we found that the temperature relation based on the dereddened Strömgren indices from Balona (1984) provides a fair agreement to our measured T_{eff} from the TLUSTY model fits for B stars with $T_{\text{eff}} > 15,000 \text{ K}$. A small correction factor improves the agreement. We formed a sample of temperature calibrators using the B stars in NGC 3293, NGC 4755, and NGC 6231 with $T_{\text{eff}} > 15,000 \text{ K}$ (measured from the TLUSTY models as described above) and available Strömgren photometry. We also included eight calibrators with well-known $T_{\text{eff}} > 15000 \text{ K}$ (measured from their absolute integrated stellar flux) from Napiwotzki et al. (1993). We performed a linear fit to T_{eff} and T_{Balona} and found a very similar relationship to that found in Paper 3. The photometry in WEBDA is from a number of different sources that often do not agree well, so the scatter in our temperature relation for these calibrators introduces

an error of 1300 K, much higher than we found for NGC 3766 in Paper 3.

To apply this temperature relation to the Be stars, we also need an accurate measurement of their β magnitudes, which are unreliable due to their emission at this line. As in Paper 3, we used the B star calibrators to find a linear fit to the observed (c_0, β) relation. The mean scatter between β_{fit} and the measured β is 0.017, which implies an additional error of 424 K in T_{eff} using the corrected T_{Balona} relation above.

Finally, we measured T_{eff} for all Be stars in NGC 3293, NGC 4755, and NGC 6231 with Strömgren photometry available in the WEBDA database using the adopted β_{fit} and the corrected T_{Balona} as described above. Adding the temperature errors from both fits in quadrature, we adopt a total error of 1400 K. The results for the Be stars are listed in columns 5–6 of Table 5. We found that all but one of the Be stars have $T_{\text{eff}} > 15,000$ K, and the single exception has $T_{\text{eff}} = 14,704$ K. Therefore we did not need to extend the calibration sample to include stars with lower temperatures.

The values of $\log g$ are more strongly dependent on β , so we were reluctant to use our β_{fit} with the Strömgren relation for $\log g$ given by Balona (1984). Instead, we used the calculated T_{eff} to determine the Be stars’ bolometric corrections, BC, from Lanz & Hubeny (2007), at first assuming $\log g = 4.0$. We calculated each stellar radius, R_* , and luminosity, L_* , using the measured T_{eff} , BC, V magnitude, distance modulus $(V - M_V)_0$, and $E(B - V)$. The adopted $(V - M_V)_0$ are listed in Table 4. We measured the stellar mass, M_* , from the computed T_{eff} and L_* by interpolating between the evolutionary tracks of Schaller et al. (1992). Finally, we obtained a preliminary value of $\log g$ from M_* and R_* . Since the BC is weakly dependent on $\log g$, we improved the BC from the initial estimate and iterated to compute the final $\log g$. We adopt a formal error in $\log g$ computed from ΔT_{eff} and the quoted errors in $(V - M_V)_0$ and $E(B - V)$.

We note that the evolutionary tracks of Schaller et al. (1992) do not account for rotation, especially the very fast rotation observed among the Be stars. Evolutionary tracks that include fast rotation reveal differences (sometimes very substantial) in the luminosity and MS lifetime of rapidly

rotating stars (e.g., Ekström et al. 2008). However, the photometric magnitudes and colors of Be stars in our work are likely contaminated by enhanced bound-free and free-free emission from the circumstellar disks. Carciofi et al. (2006) showed that the V magnitude of the Be star δ Sco increased by 0.7 magnitudes during a recent disk outburst. However, they also found that the emission line strength and visual brightness in δ Sco are sometimes anticorrelated, possibly due to changes in the mass loss rate or disk geometry. The uncertainty in V combined with the large errors in our measured T_{eff} for the Be stars in this work negate any advantage in using evolutionary tracks for fast rotating stars. Therefore we apply the Schaller et al. models throughout this work.

As we found in Paper 3, the agreement is very good between the Strömgren $\log g$ and $\log g_{\text{polar}}$ for the nonemission B-type calibrators, so we do not perform any further correction to obtain $\log g_{\text{polar}}$ for the Be stars. However, several effects may cause the Be stars to appear slightly more evolved and artificially brightened. Scattered light and continuum emission from the disk can increase the apparent brightness, an effect that is nearly impossible to correct without detailed knowledge of the disk geometry and orientation. Rotational mixing in these rapid rotators can enrich the hydrogen-burning core and increase their luminosity during their evolution (Heger & Langer 2000; Meynet & Maeder 2000; Ekström et al. 2008). On the other hand, the rapid rotation will also decrease the surface temperature at the stellar equator (the Von Zeipel effect; von Zeipel 1924), and depending on the orientation, the flux may decrease. We consider the values of $\log g_{\text{polar}}$ to be lower limits, and our measurements of R_* upper limits, for the Be stars. The final parameters for these Be stars are listed in Table 5.

5. The Be and B Star Populations

5.1. Rotational Velocity Distributions

The cumulative $V \sin i$ distribution for all Be and normal B-type stars in NGC 3293, NGC 3766, NGC 4755, and NGC 6231 are shown in Figure 6, and we find that all four are very similar. To test the null hypothesis that the distributions differ, we used the two-sided Kolmogorov-Smirnov (K-S) statistical test with all six permutations of pairs of

cluster data. The K-S test indicates that no single cluster has a significantly different distribution of $V \sin i$. The known and candidate SB systems may have overestimated measurements of $V \sin i$ due to line blending, but they do not influence the relative distributions of the clusters' $V \sin i$. We measure a mean $V \sin i = 184 \text{ km s}^{-1}$ with a standard deviation of 90 km s^{-1} for the normal B-type stars, including the SB systems.

A number of environmental factors may influence rotational velocities among cluster members: the ages, binary fraction, and magnetic fields. Huang & Gies (2006, 2008) find that the most massive B-type stars spin down with age as predicted by models due to their radial expansion and angular momentum lost by stellar winds. Since the four clusters we observed have nearly identical ages (Paper 2), we are not surprised that their $V \sin i$ distributions are very similar. Binary systems are expected to spin down faster than single star systems due to tidal synchronization processes (Abt et al. 2002), and Huang & Gies (2006) found a sharp decline in $V \sin i$ for binaries in which the more massive component has $\log g_{\text{polar}} \leq 3.9$. The cluster NGC 6231 has a very high binary fraction of at least 52% among its B-type stars (Raboud 1996) and at least 63% among O-type stars (Sana et al. 2008), so many of our targets are likely binaries that will lose angular momentum due to tidal interactions as they evolve. However, most of our targets have $\log g_{\text{polar}} > 4.0$ and do not appear to have reached synchronization. Finally, Huang & Gies (2006) found that intermediate and low mass B stars spin down faster than more massive B-type stars, possibly due to additional angular momentum losses such as magnetic fields. Indeed, two magnetic B stars were recently detected in NGC 3766 (McSwain 2008). The similarity in the $V \sin i$ distributions in NGC 3293, NGC 3766, NGC 4755, and NGC 6231 suggests that the environments are very similar or that the clusters are too young for the various environmental factors to produce observable differences in rotation.

Since we find no systematic differences among the cluster $V \sin i$ distributions, we can explore trends in $V \sin i$ for the combined Be star populations. We have measured $V \sin i$ for 12 Be stars with relatively steady-state disks (emission present in each of our observations) and 17 Be stars with significant changes in their disk emis-

sion state (either outbursts or disk fading events). The mean $V \sin i$ and its standard deviation for the stable (transient) Be stars is $263 \pm 66 \text{ km s}^{-1}$ ($253 \pm 74 \text{ km s}^{-1}$). Figure 7 shows the cumulative distribution of $V \sin i$ for the Be stars with stable disks and transient disks compared to the normal B-type cluster population. The K-S test indicates a relatively high probability (46%) that the transient and stable Be stars have the same $V \sin i$ distribution, so the differences in their distributions are not significant. For the combined Be star sample, the K-S test indicates only a 0.03% probability that their $V \sin i$ are drawn from the same distribution as the normal B-type stars. Both the stable and transient Be stars are clearly populations of rapid rotators compared to the normal B-type stars in the sample, in excellent agreement with several other recent studies of Be rotation (Hunter et al. 2008; Martayan et al. 2006; Martayan et al. 2007; Paper 3).

5.2. T_{eff} and $\log g$ Distributions

In Figures 8–11, we plot the T_{eff} and $\log g$ distributions for each cluster with the corresponding evolutionary tracks for nonrotating stars from Schaller et al. (1992).

The large population of Be transients with $15000 < T_{\text{eff}} < 20000 \text{ K}$ in NGC 3766 is striking, but we doubt that this is significant. Due to the cluster's older age, its members are more evolved and are generally not found at higher temperatures. In addition, nearly every Be transient in the other three clusters lies outside this range, and the transients are well distributed among the entire observed range of temperatures. The relationship between transients and cluster age is not clear, and it is worth investigating the transient Be star phenomenon in more clusters to determine whether there is an evolutionary dependence.

Like the transient Be stars, the stable Be stars are equally distributed over the entire temperature range. There is no clear dependence in T_{eff} and $\log g$ that distinguishes the stable Be stars from the transients or normal B-type star populations.

6. Summary

From H α spectroscopy of 296 stars in 8 open clusters, we have identified a total of 23 Be stars that experience transitions from the Be to B spec-

troscopic phase (including those in NGC 3766 that we reported in Paper 3). We also find 22 Be stars that have relatively stable disks that are consistently present in our multiple epochs of H α spectroscopy. Transient Be stars do not appear equally common in the open clusters, and we find higher rates of disk appearance and disappearance events in Collinder 272, Hogg 16, NGC 3766, and NGC 6231. These clusters will be important sites to study the disk dissipation and formation mechanisms for Be stars.

From blue optical spectroscopy and available Strömgren photometry of 128 Be and B-type stars in 4 open clusters, we have measured the T_{eff} , $\log g_{\text{polar}}$, and $V \sin i$ of these stars. Our sample of physical parameters includes 17 transient Be stars and 12 stable Be stars, and we compare their rotational properties to find that all of the Be stars have a similar distribution of $V \sin i$ and are more rapidly rotating than normal B-type stars. Other than the temporary disappearance of their disk emission, the transient Be stars do not exhibit significant physical differences from Be stars with relatively stable disks.

We are grateful to the anonymous referee for comments that greatly improved this manuscript. We thank the staff at CTIO, especially Knut Olsen and all of the night assistants, for their hard work and patient support during our many observing runs. Support for MVM has been provided by an NSF Astronomy and Astrophysics Postdoctoral Fellowship and by an institutional grant from Lehigh University. This material is based upon work supported by the National Science Foundation under Grants No. AST-0606861, AST-0507219, and AST-0401460.

Facility: CTIO:4m (Hydra)

REFERENCES

- Abt, H. A., Levato, H., & Grosso, M. 2002, ApJ, 573, 359
- Balona, L. A. 1984, MNRAS, 211, 973
- Carciofi, A. C., et al. 2006, ApJ, 652, 1617
- Dufton, P. L., et al. 2006, A&A, 457, 265
- Ekström, S., Meynet, G., Maeder, A., & Barblan, F. 2008, A&A, 478, 467
- García, B., & Mermilliod, J. C. 2001, A&A, 368, 122
- Grundstrom, E. D., & Gies, D. R. 2006, ApJ, 651, L53
- Heger, A., & Langer, N. 2000, ApJ, 544, 1016
- Huang, W., & Gies, D. R. 2006, ApJ, 648, 591
- Huang, W., & Gies, D. R. 2008, ApJ, 683, 1045
- Hunter, I., Lennon, D. J., Dufton, P. L., Trundle, C., Simón-Díaz, S., Smartt, S. J., Ryans, R. S. I., & Evans, C. J. 2008, A&A, 479, 541
- Kurucz, R. L. 1994, Kurucz CD-ROM 19, Solar Abundance Model Atmospheres for 0, 1, 2, 4, 8 km/s (Cambridge: SAO)
- Lanz, T., & Hubeny, I. 2003, ApJS, 146, 417
- Lanz, T., & Hubeny, I. 2007, ApJS, 169, 83
- Martayan, C., Floquet, M., Hubert, A. M., Gutiérrez-Soto, J., Fabregat, J., Neiner, C., & Mekkas, M. 2007, A&A, 472, 577
- Martayan, C., Frémat, Y., Hubert, A.-M., Floquet, M., Zorec, J., & Neiner, C. 2006, A&A, 452, 273
- Mathew, B., Subramaniam, A., & Bhatt, B. C. 2008, MNRAS, 388, 1879
- McSwain, M. V. 2008, ApJ, 686, 1269
- McSwain, M. V., & Gies, D. R. 2005a, ApJ, 622, 1052 (Paper 1)
- McSwain, M. V., & Gies, D. R. 2005b, ApJS, 161, 118 (Paper 2)
- McSwain, M. V., Huang, W., Gies, D. R., Grundstrom, E. D., & Townsend, R. H. D. 2008, ApJ, 672, 590 (Paper 3)
- Meilland, A., Stee, P., Zorec, J., & Kanaan, S. 2006, A&A, 455, 953
- Meynet, G., & Maeder, A. 2000, A&A, 361, 101
- Napiwotzki, R., Schoenberner, D., & Wenske, V. 1993, A&A, 268, 653
- Perry, C. L., Hill, G., & Christodoulou, D. M. 1991, A&AS, 90, 195

- Porter, J. M., & Rivinius, T. 2003, *PASP*, 115, 1153
- Raboud, D. 1996, *A&A*, 315, 384
- Sana, H., Gosset, E., Nazé, Y., Rauw, G., & Linder, N. 2008, *MNRAS*, 386, 447
- Sana, H., Gosset, E., Rauw, G., Sung, H., & Vreux, J.-M. 2006, *A&A*, 454, 1047
- Schaller, G., Schaerer, D., Meynet, G., & Maeder, A. 1992, *A&AS*, 96, 269
- von Zeipel, H. 1924, *MNRAS*, 84, 665
- Wisniewski, J. P., & Bjorkman, K. S. 2006, *ApJ*, 652, 458

TABLE 1
JOURNAL OF SPECTROSCOPY

UT Dates	Range (Å)	Resolving Power ($\lambda/\Delta\lambda$)	Slit Plate (μm)	Grating/Order	Filter	Targets
2005 Feb 2 – 3	4100 – 6900	1900	200	KPGL3/1	...	Collinder 272, IC 2581, NGC 3293, NGC 3766, NGC 4755
2006 May 13	3790 – 4708	3170	...	KPGLD/2	BG39	NGC 3766, NGC 6231
2006 May 14 – 15	5125 – 8000	1560	...	KPGL3/1	...	Collinder 272, NGC 3293, NGC 3766, NGC 6231, NGC 6664
2007 May 3 – 4	3790 – 4708	4250	200	KPGLD/2	BG39	NGC 3293, NGC 3766, NGC 4755
2007 May 5 – 6	5125 – 8000	2000	200	KPGL3/1	...	Collinder 272, IC 2581, NGC 3293, NGC 3766, NGC 4755, NGC 6231, NGC 6664

TABLE 2
H α EQUIVALENT WIDTHS

Cluster, MG ID	HJD (t - 2,450,000), $W_{H\alpha}$ (Å) (2005 Feb)	HJD (t - 2,450,000), $W_{H\alpha}$ (Å) (2006 May)	HJD (t - 2,450,000), $W_{H\alpha}$ (Å) (2007 May)	Emission status in Paper 2	Emission status in this work
Collinder 272	3404.832	3870.178	4225.757
42	8.60	8.87	7.35
44	7.60	7.64	10.22
157	8.84	9.17	10.45
188	8.20	8.94	9.11
199	10.45	10.77	10.94
222	10.52	10.95	10.97
225	9.82	10.48	9.29
254	4.43	4.62	4.63
267	5.92	6.28	6.23
288	...	10.54	10.13
302	6.54	6.91	6.77
309	6.62	7.31	7.41
310	10.66	10.70	10.85
311	7.74	7.74	7.84
329	8.37	9.64	10.00
349	7.99	8.65	8.47
376	10.79	10.54	10.67
377	7.50	8.40	8.27
397	8.93	9.20	8.58
406	...	13.00	12.36
448	10.47	8.92	9.21
484	12.58	9.13
508	-42.93	-38.08	...	Be	Be
513	-6.90	-2.73	-0.46	Be?	Be
560	10.33	10.08	10.32	Be?	...
561	9.00	8.65	8.62
562	-4.56	-1.70	2.92	Be?	Be transient
565	10.23	10.52	...	Be	...
621	1.01	4.90	8.43	...	Be transient
665	7.08	7.34	7.84
678	...	6.79	7.27
708	...	10.59	10.45
717	6.80	7.74	7.62
755	11.67	11.49	11.44
767	7.71	10.94	7.52	Be	Be transient
793	...	11.71	10.97
Hogg 16	3404.832	3870.178	4225.757
94	8.10	8.26
125	4.44	4.55	3.93
134	12.03	11.61
154	8.47	8.55
185	1.69	5.54	2.69	...	Be transient
209	4.32	4.54	4.21
217	12.16	12.14	14.34
227	...	5.40
254	...	13.17
317	4.43	5.05	4.77
IC 2581 ^a	3404.708	...	4225.5494
5	8.72	...	11.07
9	9.22	...	10.04
10	5.87	...	6.05	Be?	...
19	6.91	...	7.27
27	11.12	...	11.77
42	7.54	...	7.21
44	5.84	...	6.40

TABLE 2—*Continued*

Cluster, MG ID	HJD (t - 2,450,000), $W_{H\alpha}$ (Å) (2005 Feb)	HJD (t - 2,450,000), $W_{H\alpha}$ (Å) (2006 May)	HJD (t - 2,450,000), $W_{H\alpha}$ (Å) (2007 May)	Emission status in Paper 2	Emission status in this work
48	7.05	...	7.21
73	12.96	...	11.93
84	9.46	...	10.35
99	10.08	...	11.34
105	10.31	...	10.76
113	8.40	...	10.48	...	Be transient
119	4.05	...	4.34
122	4.06	...	5.65
123	5.80	...	7.10	Be?	...
153	4.53	...	4.92
157	6.52	...	7.11	Be?	...
158	-14.88	Be	Be
173	8.59	...	8.43
179	7.24	...	7.74
181	7.09	...	7.30
188	6.99	...	7.83
210	2.80	...	3.35
216	9.10	...	9.38
219	3.06	...	6.90	Be?	...
233	7.74	...	8.57
243	-48.51	...	-46.44	Be	Be
247	7.07	...	7.46
251	3.69	...	3.97
267	0.88	...	1.05	Be?	...
270	5.13	...	6.64	Be?	...
277	7.54	...	7.55
295	3.90	...	4.07
298	7.21
314	8.97	...	9.29
316	9.32	...	9.24
323	7.25	...	6.27	Be?	...
329	6.24	...	6.34
370	9.41	...	9.57
NGC 3293 ^a	3404.772	3870.506	4223.321
1	6.02	5.43	4.92
2	5.47	5.22	4.68
4	4.24	3.29	-0.60	Be?	...
7	8.10	7.87	7.05
8	4.75	4.67	4.07	Be?	...
9	5.64	6.27
16	9.08	9.37	9.05
18	9.27	8.85
22	4.35	4.43	4.50
23	4.18	6.14	6.12
27	6.02	6.26	6.10	Be?	...
28	3.96	4.20	4.20
40	3.51	4.10	4.16
42	-1.60	-1.48	-2.26	Be	Be
46	2.14	2.83	2.72	Be	Be
47	3.32	3.70	3.86
51	4.58	5.68	4.67	Be?	...
54	6.57	5.06	4.23	Be?	...
61	6.03	5.94	5.27
62	3.52	3.73	3.88
67	6.18	6.39	6.12
74	2.56	3.83	4.16	...	Be transient
83	0.47	4.14	4.15	...	Be transient

TABLE 2—*Continued*

Cluster, MG ID	HJD (t - 2,450,000), $W_{H\alpha}$ (Å) (2005 Feb)	HJD (t - 2,450,000), $W_{H\alpha}$ (Å) (2006 May)	HJD (t - 2,450,000), $W_{H\alpha}$ (Å) (2007 May)	Emission status in Paper 2	Emission status in this work
84	7.22	7.31	7.34	Be?	...
90	4.09	4.08	4.27
95	3.20	3.84	3.97
99	-11.99	-15.89	-20.47	Be?	Be
100	3.35	3.26	3.65
107	7.74	8.78	9.01
110	3.89	5.19	5.23
120	5.57	5.66	5.63
NGC 3766	3403.790	3870.224	4225.662
2	3.24	4.07	4.11
8	6.44
16	4.28	4.26	4.39
23	9.22	9.37	9.17
25	3.18	5.30	1.54	...	Be transient
26	5.46
27	5.38	5.69	5.59
28	6.38
29	4.47
31	3.99	0.57	-6.42	...	Be transient
33	4.86
36	8.46	8.56	8.43
40	5.80
41	4.88	5.28	5.02
42	6.07	6.02	5.85
45	4.98	5.10	4.35
46	5.49
47	-11.33	-11.29	-6.43	Be	Be
49	4.37	4.89	4.70
52	4.61
54	5.18	5.61	5.31
55	5.03	5.12	5.25
57	5.67	5.86	5.66
61	4.09	4.20	4.24	Be?	...
69	2.89	3.19	3.16
72	8.27	8.65	7.08
73	0.42	3.28	0.06	Be?	Be transient
77	4.61	5.72	5.50
83	4.07	0.84	2.93	Be?	Be transient
87	5.35
89	5.70
92	2.31	2.73	3.79	Be?	Be transient
94	5.94	5.91	5.86	Be?	...
96	6.39	6.87	7.53
98	3.10	0.21	4.14	...	Be transient
101	7.40	7.44
103	5.21
109	5.10
110	4.83
111	4.56
118	7.40	7.03	6.73
119	-5.48	-3.19	-8.67	...	Be transient
121	6.54
126	7.46	8.49	7.74	Be?	...
127	-4.95	-4.00	-5.03	Be	Be
129	8.66	7.94	7.96
130	2.00	5.04	5.09	Be?	Be transient
131	5.30

TABLE 2—*Continued*

Cluster, MG ID	HJD (t - 2,450,000), $W_{H\alpha}$ (Å) (2005 Feb)	HJD (t - 2,450,000), $W_{H\alpha}$ (Å) (2006 May)	HJD (t - 2,450,000), $W_{H\alpha}$ (Å) (2007 May)	Emission status in Paper 2	Emission status in this work
133	-1.15	-9.14	-12.72	...	Be transient
137	6.02
138	5.09
139	5.46	4.24	5.05	Be?	Be transient
142	6.57
145	7.43
148	4.84
149	7.55
150	6.83
154	-40.07	-33.56	-33.40	Be	Be
155	7.92	7.90	7.42
161	3.92	4.19	4.18
162	9.15	9.23	8.85
164	6.46
170	4.81	5.26	5.34
171	5.11
173	7.79	7.92	7.80
175	6.67	6.74	6.64
176	3.54
178	6.32	7.71	7.40
179	4.25
184	5.72
190	6.81	6.86
192	6.87
196	4.32	4.39	1.69	...	Be transient
197	7.65	8.85	8.49
198	-43.40	-53.71	-53.96	Be	Be
200	-6.66	-4.62	-5.08	Be	Be
NGC 4755	3403.863	...	4223.717
1	6.31	...	6.63
6	9.50	...	10.33
15	4.53	...	4.96
18	7.42	...	2.57	...	Be transient
25	3.59	...	4.08
27	9.94	...	11.11
30	9.61
31	4.85	...	-2.09	...	Be transient
43	7.86	Be	...
45	6.02	...	6.51
47	5.48	...	6.42
53	2.31	...	2.69	Be?	...
54	9.35	...	10.06
71	5.01	...	5.80
73	8.33	...	9.11
75	5.95	...	6.56
93	5.85	...	6.79
103	4.26	...	5.35
120	5.20	...	5.99
121	4.42	...	6.23
129	-48.80	...	-53.35	Be	Be
131	6.03	Be?	...
144	8.54	...	9.00
148	6.48	...	6.99
152	10.70	...	11.37
166	10.81	...	11.60	Be?	...
168	9.51	Be?	...
169	4.99

TABLE 2—*Continued*

Cluster, MG ID	HJD (t - 2,450,000), $W_{H\alpha}$ (Å) (2005 Feb)	HJD (t - 2,450,000), $W_{H\alpha}$ (Å) (2006 May)	HJD (t - 2,450,000), $W_{H\alpha}$ (Å) (2007 May)	Emission status in Paper 2	Emission status in this work
171	-55.57	...	-55.68	Be	Be
172	3.50	...	4.20
180	-44.23	...	-36.48	Be	Be
183	4.11	...	4.52
187	-14.19	...	-13.86	Be	Be
195	2.47	...	3.12
205	5.53
215	5.58
222	8.27	...	8.23	Be?	...
223	11.81	...	11.08	Be?	...
252	5.08
261	8.13	...	8.47
NGC 6231	...	3869.828	4223.813
2	...	5.29	4.78	Be?	Be transient
4	...	8.42	8.14
15	...	6.44	5.94
32	...	4.37	4.38
38	...	8.38	8.20
45	...	5.75	5.53
55	...	5.62	5.35
57	...	8.42	7.77
63	...	7.15	7.16
67	...	6.05	5.59	Be	...
79	...	-5.46	...	Be	Be
86	...	8.24	7.43
90	...	3.82	3.17	...	Be transient
91	...	5.18	4.97
92	...	9.82	8.32
110	...	4.57	4.48
111	...	4.27	4.22
114	...	6.48	5.74
116	...	4.46	4.49
121	...	7.52	7.04
124	...	4.49	4.43
132	...	3.98	4.03
137	...	4.12	4.04
156	...	8.94	8.38
162	...	3.14	3.23
165	...	3.27	3.39
168	...	3.94	3.95
169	...	6.34	5.99
178	...	6.87	6.98
185	...	7.82	7.12
190	...	3.52	3.49
213	...	6.32	6.19
218	...	4.14	4.11
221	...	6.71	6.96	Be?	Be transient
235	...	7.06	6.97
245	...	5.65	5.67
268	...	7.49	7.96
NGC 6664	...	3870.933	4223.930
5	11.20
13	...	6.88	6.82
33	...	8.09	7.84
35	...	6.55	6.28
45	...	10.20	10.32

TABLE 2—*Continued*

Cluster, MG ID	HJD (t - 2,450,000), $W_{H\alpha}$ (Å) (2005 Feb)	HJD (t - 2,450,000), $W_{H\alpha}$ (Å) (2006 May)	HJD (t - 2,450,000), $W_{H\alpha}$ (Å) (2007 May)	Emission status in Paper 2	Emission status in this work
53	...	8.19	8.26
62	...	7.24	7.12
68	...	8.90	8.89
73	...	5.82	5.79
79	...	3.82	3.71
81	...	12.57	12.17
119	...	6.42	6.14
126	...	1.76	2.84	...	Be
137	...	-4.32	-4.37	Be?	Be
141	...	11.41	11.15
143	...	9.50	9.00
158	...	11.35	11.45
168	...	7.82	7.59
177	...	-7.27	-7.37	Be	Be
182	...	1.47	1.74	Be	Be
183	...	7.20	7.21
207	...	6.85	6.73
219	...	5.69	5.56
221	...	-18.49	-18.68	Be	Be
229	10.48
237	...	7.13	6.84

^a $W_{H\alpha}$ may be contaminated by nebular emission in NGC 3293 and IC 2581.

TABLE 3
FRACTION OF BE TRANSIENTS

Cluster	Number of Be Stars, n	Number of Transient Be Stars, t	Ratio of Transients to Total Be, p (%)
Collinder 272/Hogg 16	6	4	67 ± 19
IC 2581	3	1	33 ± 27
NGC 3293	5	2	40 ± 22
NGC 3766	16	11	69 ± 12
NGC 4755	6	2	33 ± 19
NGC 6231	4	3	75 ± 22
NGC 6664	5	0	0 ± 18

TABLE 4
CLUSTER PARAMETERS

Cluster	Photometric fitting constant, C (mag)	$E(b - y)$ (mag)	$(V - M_V)_0$ (mag)	log age (yrs)	Reference
Collinder 272	0.49 ± 0.06	0.34	11.55	7.11	Paper 2
Hogg 16	0.43 ± 0.08	0.31	11.00	7.05	Paper 2
IC 2581	0.51 ± 0.05	0.31	12.00	7.14	Paper 2
NGC 3293	0.31 ± 0.13	0.19	12.24	7.0	Dufton et al. (2006)
NGC 3766	0.27 ± 0.02	0.17	11.6	7.16	Paper 2, Paper 3
NGC 4755	0.43 ± 0.02	0.28	11.61	7.0	Dufton et al. (2006)
NGC 6231	0.44 ± 0.06	0.35	11.07	6.9	Perry et al. (1991), Sana et al. (2006)
NGC 6664	0.67 ± 0.06	0.56	10.70	7.66	Paper 2

TABLE 5
PHYSICAL PARAMETERS OF CLUSTER MEMBERS

Cluster	MG ID	$V \sin i$ (km s^{-1})	$\Delta V \sin i$ (km s^{-1})	T_{eff} (K)	ΔT_{eff} (K)	$\log g$	$\Delta \log g$	$\log g_{\text{polar}}$	M_* (M_{\odot})	ΔM_* (M_{\odot})	R_* (R_{\odot})	ΔR_* (R_{\odot})	V_{crit} (km s^{-1})	Comment
B stars: NGC3293	1	139	21	22100	300	4.72	0.03	4.74	6.2	0.2	1.8	1.6	668	...
	2	229	50	16528	400	4.29	0.05	4.41	4.5	0.2	2.2	0.5	512	...
	4	298	35	15050	50	4.15	0.03	4.37	3.9	0.0	2.2	0.3	482	...
	8	309	75	16636	650	3.67	0.08	4.00	5.5	0.4	3.9	0.8	424	...
	9	266	31	16218	550	4.17	0.08	4.35	4.5	0.2	2.4	0.4	493	...
	16	180	24	10665	132	4.11	0.07	4.21	2.6	0.0	2.1	0.2	397	...
	22	126	5	22750	150	2.75	0.02	3.84	10.0	0.2	6.3	1.8	448	...
	27	185	28	16640	250	4.17	0.02	4.28	4.8	0.1	2.6	0.1	482	SB2? (this work)
	28	54	6	22944	350	3.73	0.02	3.75	10.8	0.3	7.2	1.8	434	...
	40	154	7	23375	300	3.84	0.02	3.94	10.0	0.3	5.6	2.2	475	...
	47	105	9	29833	200	3.91	0.02	3.91	16.8	0.3	7.5	4.6	532	...
	51	231	45	16280	1100	4.50	0.10	4.59	4.1	0.4	1.7	1.2	553	...
54	315	28	15166	150	4.18	0.03	4.40	3.9	0.1	2.1	0.4	490	...	
61	297	54	15750	450	4.29	0.05	4.47	4.1	0.2	1.9	0.7	516	...	
67	214	14	15733	200	4.13	0.02	4.27	4.4	0.1	2.6	0.9	469	...	
84	70	10	19600	300	4.75	0.00	4.76	5.2	0.2	1.6	1.4	649	...	
90	62	13	23450	450	3.68	0.02	3.71	11.4	0.3	7.8	1.8	430	...	
95	77	10	27822	900	3.93	0.08	3.95	13.9	0.8	6.5	3.6	519	...	
100	106	10	27173	950	3.78	0.07	3.83	14.2	1.0	7.6	3.3	486	...	
107	271	44	10967	171	3.82	0.07	4.08	2.9	0.1	2.6	0.1	377	...	
110	163	8	19366	200	4.02	0.03	4.13	6.6	0.1	3.7	1.4	477	...	
120	313	30	15650	250	3.97	0.02	4.24	4.5	0.1	2.7	0.9	461	...	
NGC3766	2	307	4	17071	450	3.10	0.05	3.57	7.0	0.3	7.2	0.6	352	...
	16	144	7	19420	300	3.48	0.02	3.62	8.6	0.2	7.5	0.5	380	...
	27	287	6	16033	200	3.83	0.02	4.10	4.9	0.1	3.3	0.8	436	...
	29	288	12	20140	950	4.66	0.10	4.72	5.6	0.4	1.7	1.7	645	...
	33	257	27	16828	350	4.10	0.05	4.28	4.9	0.1	2.6	0.2	484	...
	36	283	22	11931	145	4.02	0.05	4.27	3.0	0.0	2.1	0.1	424	...
	41	84	7	17900	300	3.78	0.03	3.84	6.6	0.1	5.1	0.8	406	...
	42	239	5	16100	100	3.90	0.02	4.11	4.9	0.0	3.2	0.8	438	...
	45	90	28	15500	550	4.61	0.02	4.64	3.6	0.3	1.5	1.0	554	...
	46	272	27	15530	550	4.52	0.03	4.64	3.7	0.3	1.5	1.0	554	...
	49	252	9	17400	100	3.75	0.02	3.99	6.0	0.1	4.1	0.9	431	...
	54	192	9	17340	250	3.82	0.02	3.99	5.9	0.1	4.1	0.9	430	...
55	121	6	18000	200	3.78	0.03	3.88	6.6	0.1	4.9	0.8	413	...	
57	238	8	16760	250	3.98	0.03	4.17	5.1	0.2	3.1	1.0	459	...	
61	331	8	18883	350	3.23	0.05	3.71	7.7	0.3	6.4	0.6	390	SB2? (Paper 3)	
77	338	10	16000	200	3.80	0.05	4.15	4.8	0.1	3.1	0.9	445	...	
89	189	36	11714	665	4.33	0.21	4.39	2.7	0.2	1.7	0.9	447	...	
94	177	4	15650	150	3.78	0.03	3.94	5.0	0.1	4.0	0.5	401	...	
96	121	5	13937	171	4.31	0.04	4.37	3.6	0.1	2.0	0.3	472	...	

TABLE 5—Continued

Cluster	MG ID	$V \sin i$ (km s^{-1})	$\Delta V \sin i$ (km s^{-1})	T_{eff} (K)	ΔT_{eff} (K)	$\log g$	$\Delta \log g$	$\log g_{\text{polar}}$	M_{\star} (M_{\odot})	ΔM_{\star} (M_{\odot})	R_{\star} (R_{\odot})	ΔR_{\star} (R_{\odot})	V_{crit} (km s^{-1})	Comment
	101	309	14	12753	192	3.84	0.05	4.14	3.5	0.1	2.6	0.4	409	...
	109	86	6	17100	200	4.22	0.03	4.26	5.0	0.1	2.7	1.1	483	...
	110	50	13	16060	750	4.50	0.08	4.51	4.2	0.3	1.9	0.9	531	...
	111	66	9	18436	450	4.25	0.05	4.28	5.7	0.2	2.9	0.2	503	...
	118	242	9	13353	191	3.89	0.05	4.11	3.7	0.1	2.8	0.5	409	...
	126	83	9	12399	318	3.79	0.09	3.87	3.8	0.1	3.7	0.4	358	...
	129	97	27	12034	203	3.77	0.06	3.87	3.7	0.1	3.7	0.3	355	...
	131	250	23	12817	947	4.58	0.27	4.69	2.6	0.3	1.2	1.9	526	...
	155	231	11	12694	153	4.05	0.04	4.22	3.3	0.1	2.3	0.5	425	...
	161	73	7	18400	250	3.43	0.02	3.49	8.3	0.2	8.5	0.4	351	...
	162	194	11	11513	148	3.99	0.03	4.12	3.0	0.1	2.5	0.2	390	...
	170	65	6	18060	250	3.78	0.03	3.82	6.8	0.1	5.3	0.7	403	...
	173	171	7	14210	192	4.21	0.04	4.30	3.8	0.1	2.3	0.1	459	...
	175	252	13	13823	193	4.01	0.05	4.21	3.8	0.1	2.5	0.6	435	...
	176	54	7	21435	550	4.16	0.05	4.18	7.6	0.3	3.7	1.9	510	...
	178	160	12	12504	141	3.92	0.04	4.05	3.5	0.1	2.9	0.3	390	...
	197	198	15	12402	182	4.15	0.06	4.25	3.2	0.1	2.2	0.5	427	SB? (Paper 3)
NGC4755	1	164	50	15150	150	4.09	0.02	4.20	4.3	0.1	2.7	0.8	447	...
	15	56	5	21450	350	3.87	0.03	3.89	8.6	0.2	5.5	1.6	446	...
	25	256	16	20917	900	3.32	0.08	3.32	11.9	1.1	12.5	1.8	348	...
	54	277	38	10613	85	3.74	0.04	4.02	2.8	0.0	2.7	0.1	363	...
	71	267	22	21880	1650	4.42	0.17	4.52	6.8	0.9	2.4	1.7	602	...
	75	130	14	16844	1550	4.25	0.20	4.32	4.8	0.7	2.5	0.9	493	...
	120	183	36	17495	1400	4.08	0.17	4.21	5.4	0.7	3.0	0.8	476	...
	144	173	14	10643	193	3.95	0.09	4.08	2.8	0.1	2.5	0.2	373	...
	172	57	15	23900	400	3.68	0.02	3.70	11.8	0.3	8.0	1.9	432	...
	195	69	11	27727	1350	3.61	0.12	3.63	17.5	2.0	10.6	3.3	458	...
	222	293	23	11492	232	3.90	0.08	4.18	2.9	0.1	2.3	0.3	401	...
NGC6231	15	69	10	17266	200	4.32	0.02	4.35	4.9	0.1	2.5	0.3	503	...
	32	90	9	24600	400	3.77	0.03	3.82	11.6	0.3	7.0	2.3	459	SBI? (García & Mermilliod)
	45	176	10	18100	200	4.08	0.02	4.20	5.8	0.1	3.2	1.3	481	...
	55	311	16	18250	50	4.05	0.03	4.27	5.6	0.0	2.9	0.1	500	...
	57	184	27	11119	212	3.90	0.08	4.04	3.0	0.1	2.7	0.2	372	...
	63	119	22	15450	50	4.30	0.02	4.36	4.1	0.0	2.2	0.3	486	...
	67	266	15	17733	200	4.23	0.03	4.39	5.1	0.1	2.4	0.4	518	SB (WEBDA)
	86	176	12	11703	140	3.94	0.04	4.07	3.2	0.1	2.7	0.2	385	...
	91	137	18	20700	250	3.94	0.02	4.03	7.7	0.2	4.4	1.6	469	SB (WEBDA)
	110	86	11	24690	400	4.03	0.03	4.06	10.5	0.3	5.0	2.7	515	SB2? (García & Mermilliod)
	111	402	33	24000	100	3.80	0.01	4.14	9.5	0.1	4.4	2.6	527	SB2 (García & Mermilliod)
	114	213	12	15366	200	4.02	0.02	4.18	4.5	0.1	2.8	0.8	446	...
	116	92	13	26550	850	4.23	0.08	4.25	10.9	0.6	4.1	0.5	581	SBI (García & Mermilliod)
	121	295	31	13306	304	4.04	0.07	4.29	3.5	0.1	2.2	0.2	446	...

TABLE 5—Continued

Cluster	MG ID	$V \sin i$ (km s^{-1})	$\Delta V \sin i$ (km s^{-1})	T_{eff} (K)	ΔT_{eff} (K)	$\log g$	$\Delta \log g$	$\log g_{\text{polar}}$	M_{\star} (M_{\odot})	ΔM_{\star} (M_{\odot})	R_{\star} (R_{\odot})	ΔR_{\star} (R_{\odot})	V_{crit} (km s^{-1})	Comment
	124	147	9	23850	150	3.90	0.02	3.98	10.2	0.1	5.4	2.4	490	SBI? (García & Mermilliod)
	132	164	14	28150	900	4.03	0.08	4.09	13.2	0.9	5.4	3.9	556	SB2? (this work)
	137	257	26	29194	0	3.92	0.10	4.04	14.4	0.0	6.0	4.2	553	SB2? (this work)
	156	183	19	14100	250	4.40	0.01	4.46	3.5	0.1	1.8	0.5	494	...
	162	85	13	28800	250	3.67	0.02	3.70	18.0	0.4	9.9	4.0	480	...
	165	145	25	SB2 (Sama et al. 2008)
	168	62	9	29472	550	4.15	0.05	4.16	14.0	0.5	5.2	4.4	586	...
	169	261	10	15350	50	3.80	0.00	4.05	4.7	0.0	3.4	0.7	420	...
	178	165	13	15633	350	4.34	0.06	4.41	4.1	0.2	2.1	0.6	501	...
	185	299	24	11655	185	3.72	0.06	4.03	3.2	0.1	2.9	0.2	377	...
	190	178	9	28850	150	3.60	0.00	3.73	17.7	0.2	9.6	4.1	485	...
	213	324	38	16966	200	4.12	0.03	4.35	4.8	0.1	2.4	0.3	501	...
	218	87	8	29600	100	4.25	0.02	4.26	13.5	0.1	4.5	0.1	616	SBI? (García & Mermilliod)
	235	292	62	12667	154	3.88	0.05	4.16	3.4	0.1	2.6	0.4	412	...
	245	350	12	17900	0	4.10	0.02	4.35	5.3	0.0	2.5	0.3	513	...
	268	150	21	13588	239	4.13	0.05	4.22	3.7	0.1	2.4	0.6	436	...
Be Stars:														
NGC3293														
	42	259	17	16205	1400	4.32	0.23	4.32	4.6	0.1	2.4	0.5	494	...
	46	281	9	29655	1400	3.88	0.20	3.88	16.9	0.6	7.8	1.6	524	...
	74	342	6	21338	1400	3.94	0.21	3.94	8.4	0.1	5.2	1.1	453	...
	83	365	21	21778	1400	3.84	0.21	3.84	9.0	0.1	5.9	1.2	440	...
	99	273	27	29586	1400	4.12	0.20	4.12	14.3	0.5	5.4	1.1	577	...
NGC3766														
	25	261	6	18995	301	4.02	0.09	4.02	6.6	0.1	4.2	1.2	450	...
	31	197	5	17834	400	3.82	0.10	3.99	6.2	0.2	4.2	1.0	435	...
	47	190	4	18399	301	3.30	0.09	3.30	9.3	0.4	11.3	2.5	323	...
	73	296	4	18274	301	3.49	0.09	3.49	8.2	0.2	8.5	1.3	349	...
	83	111	17	18817	301	3.31	0.09	3.31	9.8	0.4	11.5	2.4	329	...
	92	214	17	18725	301	3.34	0.09	3.34	9.5	0.4	10.9	2.2	332	...
	98	265	25	16890	301	3.84	0.10	3.84	6.2	0.2	4.9	0.6	398	...
	119	215	22	17792	301	3.75	0.09	3.75	6.8	0.1	5.8	0.5	387	...
	127	347	4	17687	550	3.61	0.12	4.01	6.1	0.3	4.0	1.0	437	...
	130	285	7	17519	301	3.69	0.09	3.69	6.9	0.1	6.2	0.4	375	...
	133	215	20	18564	301	3.53	0.09	3.53	8.3	0.2	8.2	1.0	358	...
	139	343	12	15945	301	3.95	0.10	3.95	5.2	0.2	4.0	0.5	406	...
	154	112	29	13254	1254	3.29	0.18	3.29	5.5	0.8	8.8	3.9	282	...
	196	165	4	19660	250	3.73	0.02	3.87	7.6	0.2	5.3	1.1	426	...
	198	251	6	19580	301	4.00	0.09	4.00	7.0	0.2	4.4	1.2	449	...
	200	236	12	16301	301	3.51	0.10	3.51	6.8	0.2	7.6	1.5	337	...
NGC4755														
	31	321	34	20584	1400	4.17	0.19	4.17	7.1	0.1	3.6	0.6	501	...
	129	238	24	25040	1400	3.91	0.17	3.91	11.5	0.2	6.2	1.1	483	...
	171	327	12	26246	1400	4.04	0.17	4.04	11.6	0.2	5.4	0.9	523	...

TABLE 5—*Continued*

Cluster	MG ID	$V \sin i$ (km s^{-1})	$\Delta V \sin i$ (km s^{-1})	T_{eff} (K)	ΔT_{eff} (K)	$\log g$	$\Delta \log g$	$\log g_{\text{polar}}$	M_* (M_{\odot})	ΔM_* (M_{\odot})	R_* (R_{\odot})	ΔR_* (R_{\odot})	V_{crit} (km s^{-1})	Comment
	187	16070	1400	4.23	0.21	4.23	4.7	0.1	2.8	0.5	462	...
NGC6231	2	325	23	15050	50	3.65	0.03	4.03	4.6	0.0	3.5	0.6	412	...
	79	302	32	16533	1400	4.18	0.17	4.18	4.9	0.1	3.0	0.4	456	...
	90	201	25	27117	1400	4.13	0.14	4.13	11.9	0.4	4.9	0.6	554	SB2? (García & Mermilliod)
	221	162	13	14704	1400	4.19	0.19	4.19	4.1	0.1	2.7	0.3	439	...

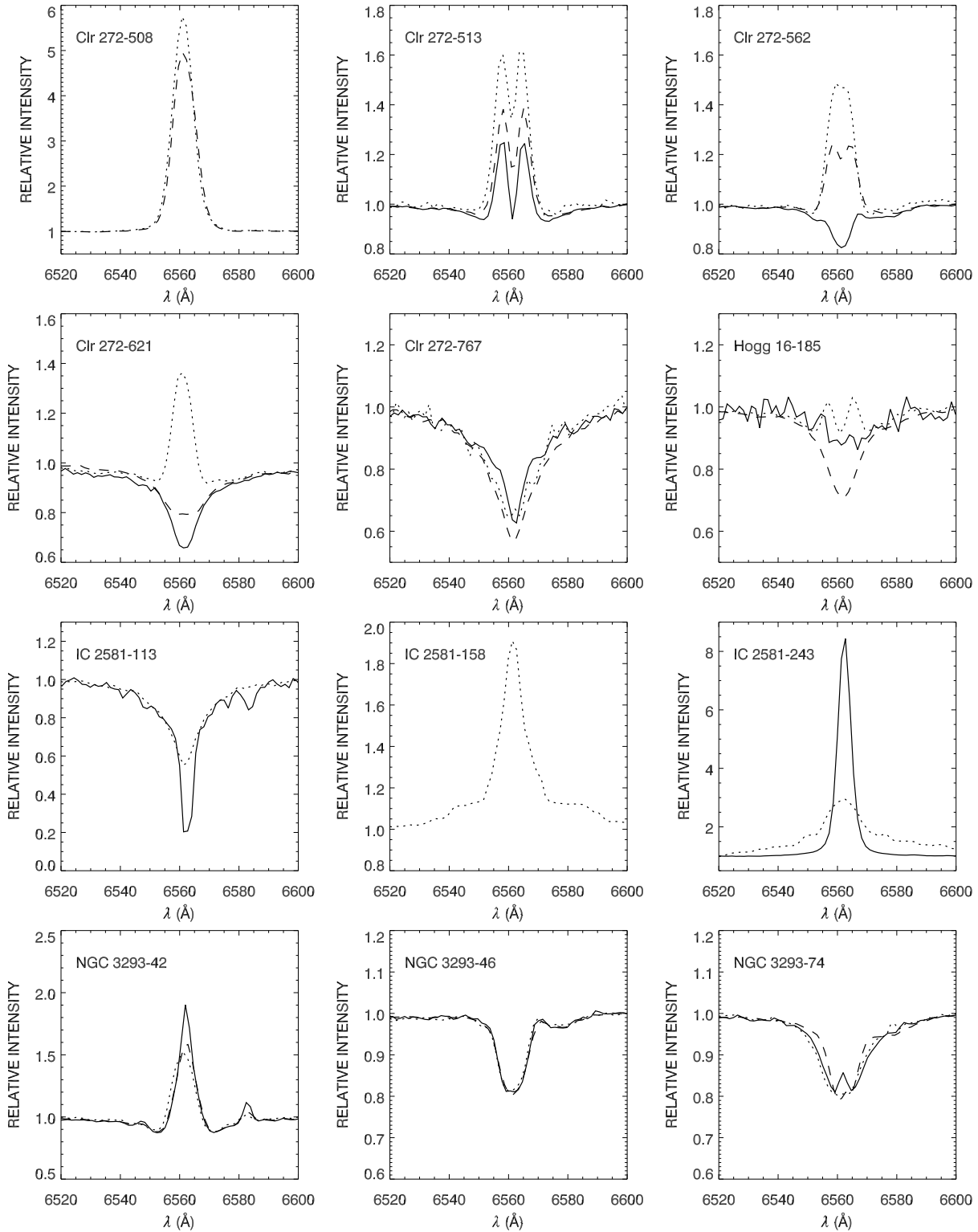


Fig. 1.— $H\alpha$ profiles of Be stars, labeled by MG ID number. Spectra from 2005, where available, are shown with dotted lines, spectra from 2006 with dashed lines, and spectra from 2007 with solid lines.

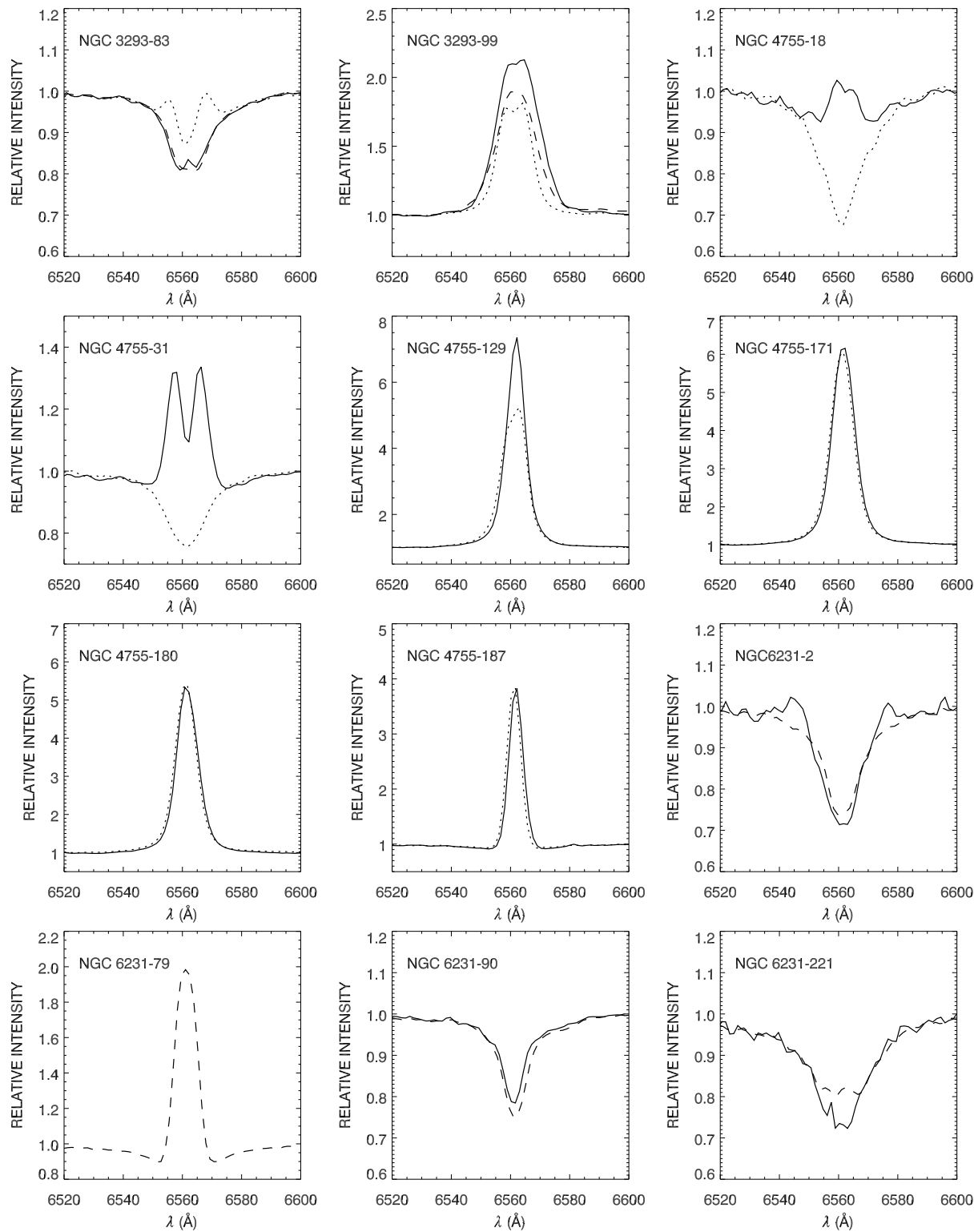


Fig. 2.— H α profiles in the same format as Fig. 1.

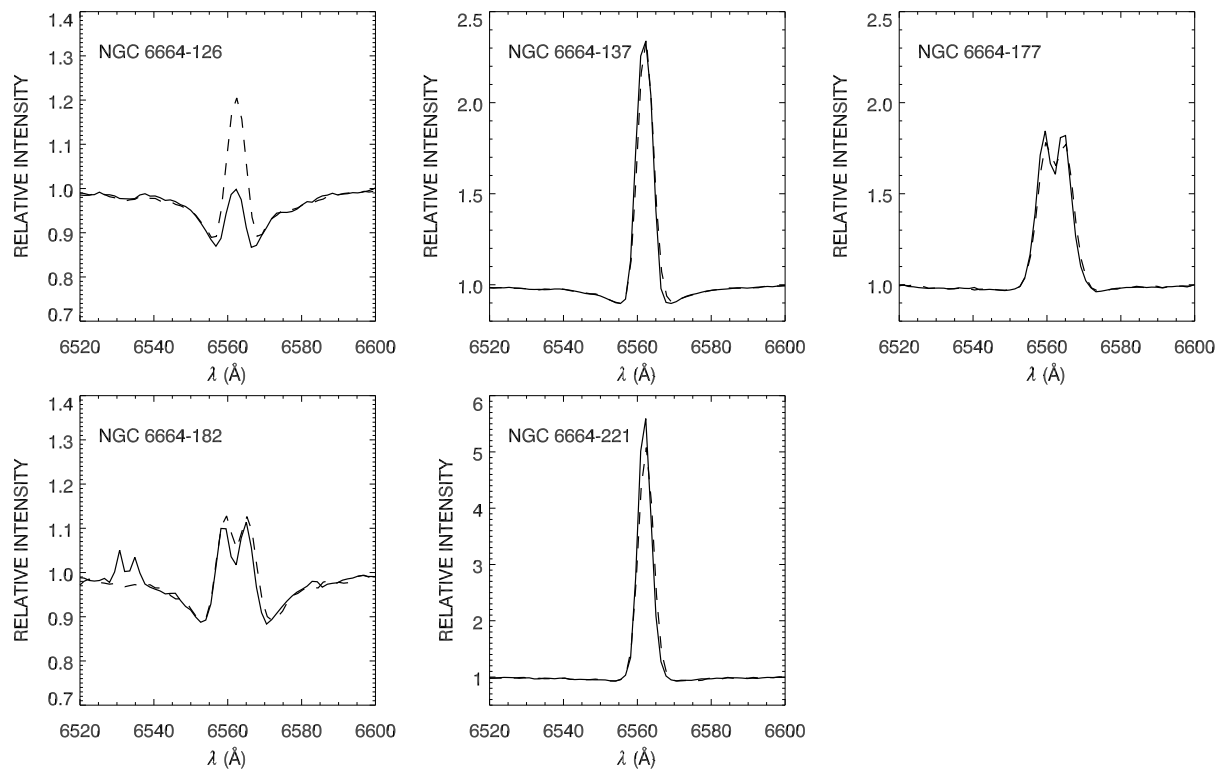


Fig. 3.— H α profiles in the same format as Fig. 1.

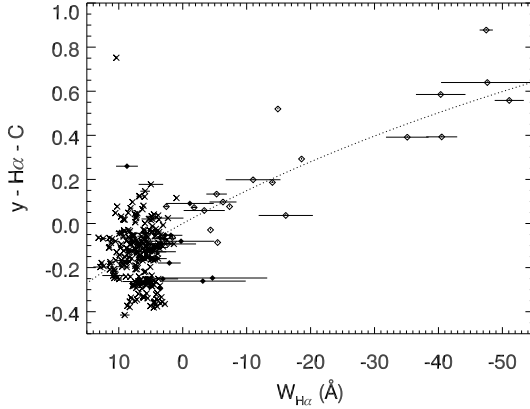


Fig. 4.— The theoretical logarithmic relationship between $W_{H\alpha}$ and $y-H\alpha$ color (*dotted line*) is shown with the mean observed $W_{H\alpha}$ and the adjusted $y-H\alpha$ color from Paper 2 for the transient Be stars (*filled diamonds*), stable Be stars (*open diamonds*), and non-emission B-type stars (*crosses*).

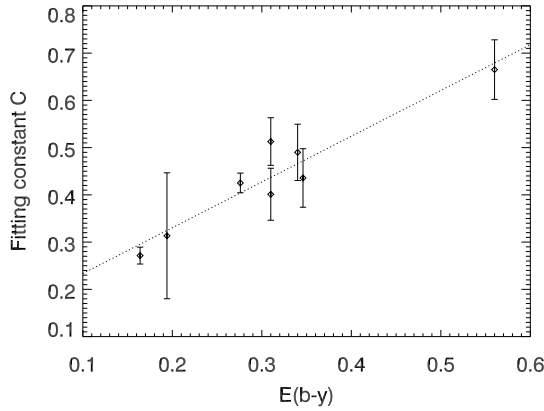


Fig. 5.— The fitting constants, C , are plotted against the clusters' reddening values, $E(b-y)$. The best fit linear relationship is also shown (*dotted line*).

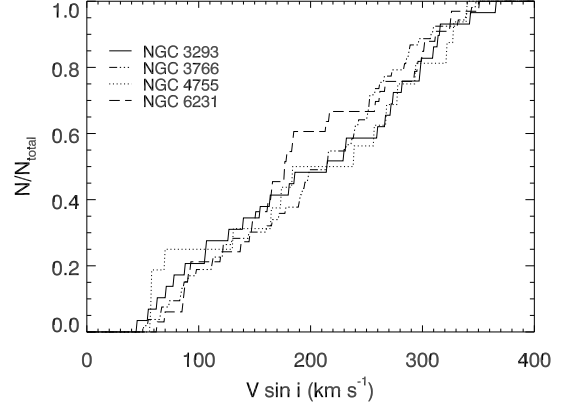


Fig. 6.— Cumulative $V \sin i$ distribution for each cluster, including both Be and normal B-type stars.

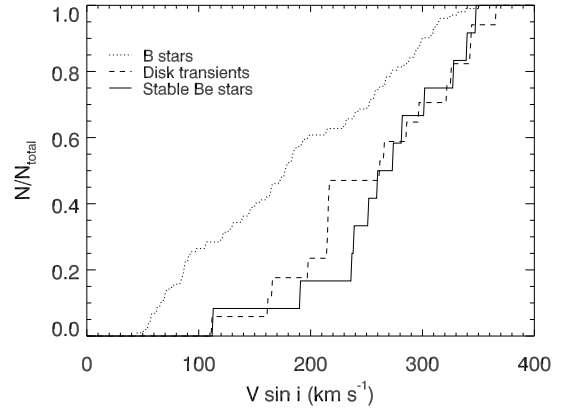


Fig. 7.— Cumulative $V \sin i$ distribution for Be stars with stable disks and those with transient disks. The distribution for normal B-type stars is also shown for reference.

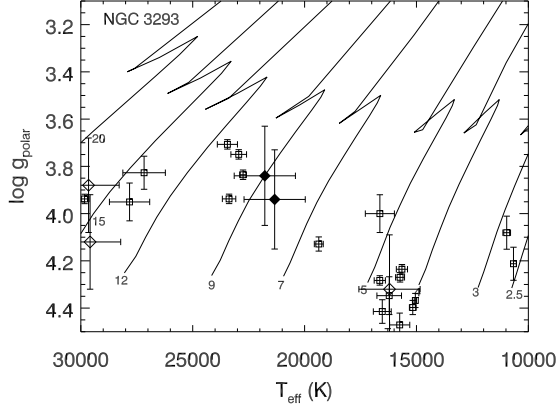


Fig. 8.— T_{eff} and $\log g$ are plotted for the cluster NGC 3293 with the evolutionary tracks of Schaller et al. (1992; *solid lines*). The ZAMS mass of each evolutionary track is labeled along the bottom. Normal B-type stars are shown as open squares, stable Be stars as open diamonds, and Be transients as filled diamonds.

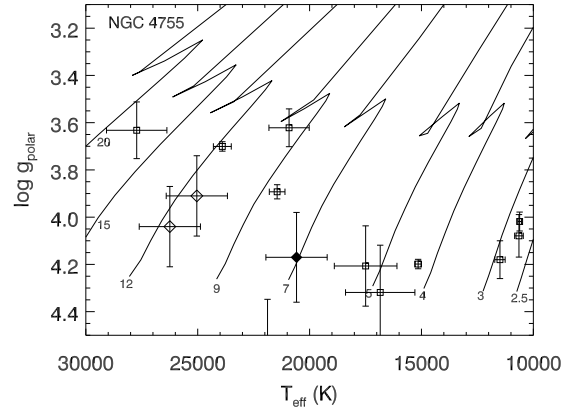


Fig. 10.— T_{eff} and $\log g$ are plotted for the cluster NGC 4755 in the same format as Figure 8.

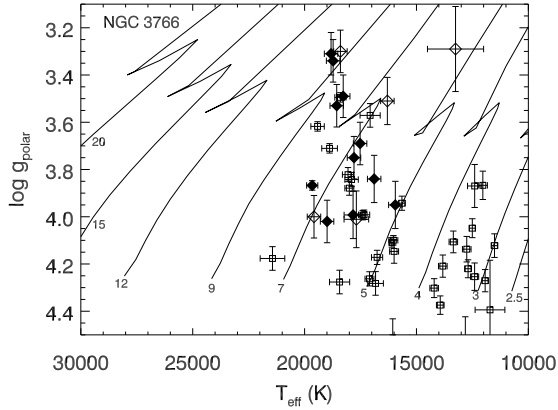


Fig. 9.— T_{eff} and $\log g$ are plotted for the cluster NGC 3766 in the same format as Figure 8.

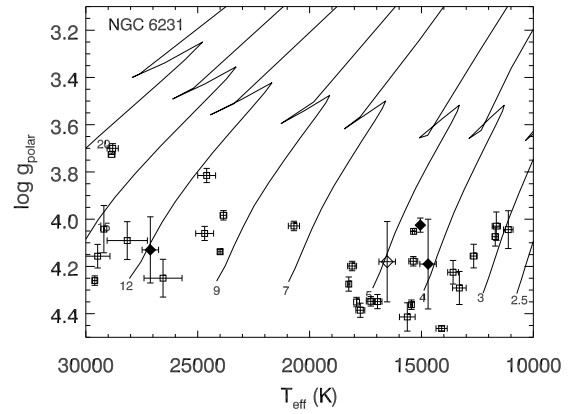


Fig. 11.— T_{eff} and $\log g$ are plotted for the cluster NGC 6231 in the same format as Figure 8.